Structural stability of hydrogenated amorphous carbon overcoats used in heat-assisted magnetic recording investigated by rapid thermal annealing

N. Wang and K. Komvopoulos*
Department of Mechanical Engineering, University of California, Berkeley, California 94720, USA

F. Rose and B. Marchon
Hitachi Global Storage Technologies, A Western Digital Company, San Jose, California 95135, USA

Abstract

Ultrathin amorphous carbon (*a*-C) films are extensively used as protective overcoats of magnetic recording media. Increasing demands for higher storage densities have necessitated the development of new storage technologies, such as heat-assisted magnetic recording (HAMR), which uses laser-assisted heating to record data on high-stability media that can store single bits in a very small area (~1 Tbit/in^2). Because HAMR relies on locally changing the coercivity of the magnetic medium by raising the temperature above the Curie temperature for data to be stored by the magnetic write field, it raises concerns about the structural stability of the ultrathin *a*-C film. In this study, rapid thermal annealing (RTA) was used to examine the thermal stability of ultrathin hydrogenated amorphous carbon (*a*-C:H) films deposited by plasma-enhanced chemical vapor deposition. Structural changes in the *a*-C:H films induced by RTA were studied by x-ray photoelectron spectroscopy, Raman spectroscopy, x-ray reflectivity, and conductive atomic force microscopy. It is shown that the films exhibit thermal stability up to a critical temperature in the range of 400–450 °C. Heating above this critical temperature, results in the depletion of hydrogen and the enhancement of sp^2 clustering. The determined critical temperature represents an upper bound of laser heating in HAMR hard-disk drives and provides a limit for the Curie temperature of magnetic materials used in HAMR.

Keywords: carbon atom hybridization, heat-assisted magnetic recording, hydrogenated amorphous carbon, rapid thermal annealing, spectroscopy, structural stability, ultrathin films

*Corresponding author: Tel: (510)-642-2563, Fax: (510)-643-5599, E-mail: kyriakos@me.berkeley.edu
Submitted to the *Journal of Applied Physics* on November 28, 2012.

I. INTRODUCTION

Thin films of amorphous carbon (*a*-C) are used in various technologies as protective overcoats because they exhibit chemical inertness, low friction, and high wear resistance.[1–3] In particular, ultrathin *a*-C films protect the magnetic medium of hard-disk drives (HDDs) against corrosion and mechanical wear caused by intermittent surface contact. The exponential increase of the storage capacity of HDDs has been largely due to the development of fine-grained magnetic media. However, data storage in very small magnetic grains (bits) is inhibited by thermal fluctuations that can easily change the magnetization direction in each bit, resulting in permanent loss of information. Although this undesirable phenomenon (known as the superparamagnetic limit) can be offset by using highly anisotropic magnetic media, the increase of the magnetic anisotropy increases the magnetic field for bit polarization above applicable levels. A promising solution to this problem is heat-assisted magnetic recording (HAMR),[4–7] which uses a tightly focused laser beam to heat and temporarily reduce the coercivity of magnetic nanodomains below that of the magnetic field applied by the head. Impulsive laser heating (typically <1 ns)[6] raises the temperature in the magnetic medium above its Curie temperature, enabling rapid data encoding by the magnetic field applied by the head. However, the intensive heating and rapid cooling raise a concern about the thermal stability of the protective carbon overcoat of HAMR disks. Therefore, knowledge of the effect of such rapidly applied thermal loadings on the integrity of the *a*-C overcoat is of great importance to the advancement of HAMR technology.

Laser heating has been shown to cause degradation of the ultrathin *a*-C overcoats used in current hard disks.[8] However, because of the very small laser spot (<100 nm in diameter when using a near-filed transducer) and short heating time in HAMR, it is difficult, if not impossible, to directly and accurately measure the temperature rise in the carbon film due to laser heating. Thus, temperature profiles for different laser heating conditions have only been obtained from numerical studies.[9] However, accurate estimation of the critical temperature for *a*-C film degradation is critical to the success of HAMR, because it determines the maximum laser power for a given magnetic medium. While a high laser power is

necessary for hearing a highly anisotropic magnetic material above its Curie temperature, it is critical that the laser power does not induce thermal degradation of the *a*-C overcoat.

Thermal annealing is a common method for studying the thermal stability of *a*-C films. Numerous thermal annealing studies have been carried out with *a*-C films deposited by different methods.[10–17] However, the films examined in these studies were significantly thicker than those used in current HDDs and the annealing time was on the order of several minutes. Initiation of hydrogen depletion and only sp^2 hybridization in radio-frequency sputtered 100-nm-thick *a*-C films annealed in vacuum have been reported to commence at a temperature of ~390 and 590 °C, respectively.[14] Tetrahedral amorphous carbon (*ta*-C) films of 70 nm thickness deposited by filtered cathodic vacuum arc (FCVA) demonstrated stress relaxation and graphitization after annealing in vacuum at 600–700 °C and 1100 °C, respectively.[15] A dependence of the thermal stability of carbon films on the method of deposition, i.e., film composition and structure, has been found in several studies.[10,12,14,15] In general, hydrogen-free *ta*-C films deposited by pulsed laser deposition (PLD)[12,16] and FCVA[17,18] exhibit higher thermal stability than other carbon films. While hydrogen-free *ta*-C films undergo graphitization during annealing in the temperature range of 700–900 °C,[15,16,17] hydrogenated amorphous carbon (*a*-C:H) films graphitize at a lower annealing temperature of ~600 °C[14] and are less stable because hydrogen depletion commences at about 300–500 °C.[14,19,20]

The objective of this study was to examine the thermal stability of ultrathin *a*-C:H films used as protective overcoats in current HDDs. To apply rapid heating typical of HAMR, *a*-C:H films deposited by plasma-enhanced chemical vapor deposition (PECVD)were subjected to thermal annealing for <1 s. Changes in the structure, carbon atom hybridization, thickness, and conductivity of the annealed *a*-C:H films were examined by visible Raman spectroscopy, x-ray photoelectron spectroscopy (XPS), x-ray reflectivity (XRR), and conductive atomic force microscopy (CAFM), respectively. Possible factors affecting the thermal stability of nanometer-thick *a*-C:H films deposited by PECVD are interpreted in the context of Raman, XPS, XRR, and CAFM results.

II. EXPERIMENTAL METHODS

Thin *a*-C:H films were deposited on 2.5-inch-diamter glass disks coated with a 96-nm-thick NiTa adhesive layer by the PECVD method, using acetylene (C_2H_2) precursor. The density of the deposited films was found to be ~2.1 g/cm^3, while the hydrogen content was estimated to be ~40%. The *a*-C:H films were exposed to various temperatures in a thermal annealing equipment, which was purged with a gas mixture of 8000 sccm N_2 and 2000 sccm O_2 to simulate atmospheric conditions.

A. Rapid thermal annealing experiments

Rapid thermal annealing (RTA) experiments were performed in a heating chamber with an integrated computer control system (RTP-600xp, Modular Process Technology). The sample holder was supported by three cantilevers with a pin at their free end. Two rows of tungsten-halogen lamps (one above and one below the sample holder) were used to heat the sample. The chamber walls were covered by a reflective coating that reduces thermal loss and enhances the temperature uniformity in the chamber during annealing. The temperature at the sample surface was measured by a thermocouple placed in contact with the backside of the sample holder. The accuracy of the temperature measurement was within 2 °C. The heating rate during RTA was set at 105 ± 8.5 °C/s. To minimize the annealing time, the time to reach a certain maximum annealing temperature was kept as short as possible. Because of the short duration of heating, the set temperature slightly differed from the real temperature measured with the thermocouple. Figure 1(a) shows a typical temperature profile during RTA obtained from thermocouple measurements. Figure 1(b) shows the difference between set and measured temperature as a function of the set temperature. Hereafter, the temperature will always refer to that measured by the thermocouple.

B. X-ray photoelectron spectroscopy and x-ray reflectivity

Because of limitations in the XPS signal intensity and XRR thickness resolution (1 Å), 9.5-nm-thick *a*-C:H films were used in the graphitization and oxidation studies. Graphitization of *a*-C films deposited by different methods commences at a temperature between 590 °C[14] and 1100 °C.[15] However, as mentioned earlier, this information has been derived from long-term annealing studies. It is unclear if

short-time annealing can also lead to graphitization. Therefore, to examine the carbon bonding configurations and detect graphitization, multiplex narrow-scan XPS spectra of the C1s core-level peak were obtained at an incident angle of 89º, measured from the sample surface. The XPS system (PHI Quantum 2000, Physical Electronics) used in this study is equipped with a monochromatic Al-Kα X-ray beam of 1486.6 eV energy and 5.7 eV work function. The energy resolution of the XPS system is 0.45 eV. XPS spectra were collected in the binding energy range of 280–295 eV under a vacuum of $<2 \times 10^{-8}$ Torr. After Shirley background subtraction, the broad C1s peaks were deconvoluted by five Gaussian distributions corresponding to sp^1, sp^2, and sp^3 hybridizations and high-order C–O and C=O bonds, respectively.[21] Binding energies of the Gaussian distributions corresponding to sp^2 and sp^3 hybridizations were set equal to 284.3 ± 0.2 and 285.2 ± 0.2 eV, respectively. The sp^3 fraction was obtained as the ratio of the distribution area corresponding to sp^3 hybridization divided by the sum of the distribution areas corresponding to sp^2 and sp^3 hybridizations.

Film oxidation under the RTA conditions of this study was examined by comparing XRR film thickness measurements obtained before and after annealing. Specular XRR data were acquired with a diffractometer (X'Pert PRO, PANalytical) equipped with a 1.8-kW, fine-focus Co ceramic x-ray tube and a graded multilayer parabolic x-ray mirror, producing an ~100-μm-wide monochromatic Co-Ka beam having a divergence of <0.04º. The experimental data were analyzed with a commercial software,[22] which determines the density, roughness, and thickness of a layered structure by finding a best fit of the experimental data using the method proposed by Parratt[23] and Névot and Croce.[24] The uncertainty in the XRR thickness measurements was estimated to be about ±1 Å.

C. Raman spectroscopy

Changes in the film structure as a result of RTA were studied with a Raman spectroscopy system (InVia, Renishaw) equipped with an Ar laser of wavelength equal to 514.5 nm. Raman spectra were recorded in the range of 950–1825 cm^{-1}. After substrate background noise subtraction, the spectra were first smoothed by a five-point Savitzky-Golay filter and then deconvoluted into two Gaussian

distributions corresponding to the D and G peaks. For statistical analysis, Raman spectra were collected from at least three different surface locations of each film before and after RTA treatment.

D. Conductive atomic force microscopy

Current images of 3.4-nm-thick *a*-C:H films were obtained before and after annealing at 660 °C with a conductive AFM system (Dimension Icon, Veeco Instruments) equipped with a tunneling module for amplifying the current signal. Film conductivity measurements were obtained by applying a bias voltage of 0, 0.2, and 1 V to the sample surface through a contacting platinum tip (Bruker) with a spring constant of 0.3 N/m and resonance frequency of 5 kHz.

III. RESULTS AND DISCUSSION

A. Film graphitization and oxidation

At an elevated temperature, carbon films may exhibit graphitization due to transformation of sp^3 carbon atom hybridization to the thermodynamically more favorable sp^2 hybridization.[11,12,16] This rehybridization decreases the film hardness and, in turn, its wear resistance. As stated earlier, previous studies dealing with the thermal stability of thick carbon films subjected to long-term thermal annealing have shown that graphitization occurs in the temperature range of 600–900 °C,[10,12,14–17] depending on the type of carbon material (deposition process). To examine whether graphitization occurred under the current RTA conditions, C1s core-level XPS spectra of 9.5-nm-thick *a*-C:H films were obtained before and after annealing at 660 °C. The similar C1s spectra of the as-deposited and annealed *a*-C:H films, shown in Fig. 2, indicate a secondary effect of RTA treatment. The sp^3 fraction before and after RTA treatment was found equal to about 8.45% and 10.15%, respectively. Because this small difference is within the error range of curve fitting, it may be inferred that RTA did not cause film graphitization.

To determine if carbon oxidation occurred during the RTA treatment, XRR measurements of the *a*-C:H film thickness were obtained before and after annealing at 660 °C. The average film thickness before and after annealing was found equal to 9.4 and 9.6 nm, respectively. Because this very small difference in film thickness is in the range of experimental error, it is concluded that RTA did not result in

film oxidation. This is attributed to the very short duration of the RTA treatment, which limited oxygen diffusion and, in turn, chemical reaction between carbon and oxygen.[25]

B. Changes in film structure

Raman spectroscopy is more sensitive to structural changes than XPS and XRR. In visible Raman spectroscopy, the photons preferentially excite the π states existing only in the sp^2 hybridizations. Consequently, this technique can indirectly yield information about the sp^3 fraction. Figure 3 shows visible Raman spectra of 3.4-nm-thick *a*-C:H films obtained before (25 °C) and after (190–658 °C) RTA treatment. For clarity, the spectra shown in Fig. 3 have been shifted upwards and fitted Gaussian distributions corresponding to the D and G peaks are only shown for the as-deposited (untreated) film. In the Raman spectrum of the untreated *a*-C:H film, the D peak centered at 1347.5 cm^{-1} is assigned to the breathing modes of the sp^2 bonds of aromatic rings, while the G peak centered at 1540.7 cm^{-1} is assigned to the bond stretching of all carbon atom pairs in the sp^2 bonds of both aromatic rings and linear chains. Thus, the presence of the D peak in the Raman spectrum can be related to aromatic ring structures.

In visible Raman spectra, both the positions and the intensities of the D and G peaks are affected by several factors, including the sp^2 cluster size, bond-length/angle disorder, sp^2 bonds in rings and chains, and sp^2/sp^3 ratio. The stretching modes of C–H bonds are between 2800 and 3100 cm^{-1}, which is outside the range of Raman analysis. The bending modes of various hydrogen configurations are between 1300 and 1600 $cm^{-1}$and are superimposed to carbon-carbon bonds. Because visible Raman spectroscopy does not induce resonance of the bending modes, the effect of these modes is usually neglected in the analysis of the Raman spectra.[26,27]

All Raman spectra shown in Fig. 3 possess similar distributions, which is expected given the very short time of RTA (<1 s at peak temperature). The only obvious difference is the slight red-shifting of the G peak with the increase of the peak temperature of annealing. This shift may be attributed to $sp^3 \rightarrow sp^2$ rehybridization, increase of sp^2 cluster size, and enhancement of sp^2 ordering in the rings.[26] However, as shown by the XPS results (Fig. 2), the RTA treatment did not affect the sp^3 content of the films. Thus, the

shift of the G peak to higher wavenumbers may be attributed to the increase of the sp^2 cluster size and sp^2 ordering in the rings.

Figure 4 shows the position and the full-width at half-maximum (FWHM) of the G peak and the D-to-G peak intensity ratio I(D)/I(G) versus the peak temperature of annealing. All plots indicate the existence of a critical temperature of about 400–450 °C, above which significant structural changes occurred in the films. As shown in Fig. 4(a), red-shifting of the G peak was greatly enhanced by the increase of the peak temperature of annealing above ~450 °C, suggesting a significant increase of the sp^2 fraction, sp^2 cluster size, chain length, and sp^2 bond ordering in the rings.[26,27] However, because the XPS results (Fig. 2) did not reveal any discernible changes in the sp^3 fraction after annealing, the significant red-shifting of the G peak above the critical temperature of annealing may be attributed to the increase of the sp^2 cluster size and the sp^2 bond ordering in the rings.

A continuous decrease of the FWHM of the G peak with increasing bond ordering has been observed in previous studies.[26,28] The FWHM of the G peak can also be correlated with the sp^2 cluster size. In particular, for visible excitation, the FWHM decreases almost linearly with increasing sp^2 cluster size, for clusters smaller than 100 nm.[28] Figure 4(b) shows that the FWHM of the G peak decreases almost linearly with the annealing temperature above ~450 °C, suggesting an increase in sp^2 cluster size and carbon atom ordering in the film.

The I(D)/I(G) ratio also correlates with the sp^2 cluster size.[29] For example, the relationship $I(D)/I(G) = 44/L_a$, where L_a is the in-plane crystallite size (expressed in Ångstroms), has been reported to hold in the range of 25 Å < L_a < 3000 Å.[30] For much smaller cluster sizes, such as those in the present *a*-C:H films, I(D)/I(G) is proportional to the probability of a six-fold ring existing in a cluster,[24] i.e., proportional to the cluster area L_a^2. Consequently, the increase of the I(D)/I(G) ratio with the annealing temperature, shown in Fig. 4(c), may be attributed to the increase of the sp^2 cluster size during RTA treatment at elevated temperatures (>450 °C).

A possible reason for the increase of the sp^2 cluster size during annealing is the depletion of hydrogen. Annealing of hydrogenated *ta*-C films in vacuum causes hydrogen depletion through the

formation of molecular H_2 at local interstitial sites, rather than hydrogen diffusion through the film, followed by H_2 effusion to the film surface.[19] Hydrogen depletion from plasma-deposited *a*-C:H films commences at a relatively low temperature (~390 °C).[14] The low density and extremely small thickness (3.4 nm) of the *a*-C:H films examined in this study were conducive to H_2 effusion to the surface. Hydrogen depletion may lead to carbon-carbon bond restructuring, accompanied by an increase in the sp^2 cluster size.[26] Although C–H modes do not affect the D and G peaks, carbon structure changes due to variations in the hydrogen content can be captured by visible Raman spectroscopy.

The G-peak positions may be affected by mechanical strain or stress relaxation in the annealed films. However, under the present RTA conditions, the *a*-C:H films were uniformly heated for a very short time without being constraint. In addition, contrary to other film deposition methods (e.g., FCVA and PLD) that use energetic carbon ions or atoms as film precursors, the residual stress in *a*-C films deposited by PECVD is relatively low.[31] Considering the aforementioned factors and the extremely small thickness of the present *a*-C:H films, it may be inferred that intrinsic (residual) stress effects on the G-peak position (Figs. 3 and 4) were insignificant.

C. Film conductivity

AFM measurements of the film conductivity provided further insight into the thermal stability of the *a*-C:H films. Figure 5 shows 500 × 500 nm CAFM images of 3.4-nm-thick *a*-C:H films obtained before (left column) and after (right column) annealing at a peak temperature of 660 °C. During CAFM imaging, the sample was grounded and the tip was biased by a voltage of 0. 0.2., and 1.0 V. Table I shows the root-mean-square current versus applied bias voltage for as-deposited and annealed 3.4-nm-thick *a*-C:H films. For a given bias voltage, the CAFM images and Table I show that the annealed *a*-C:H films produced relatively lower current intensities than the as-deposited films, indicating a detrimental effect of RTA on film conductivity. The electrical conductivity of *a*-C films can be described by a conducting electron channel model.[32] Thus, the reduced electrical conductivity of the annealed *a*-C:H films may be

attributed to the breakdown of the conductive channels through the film thickness due to the depletion of hydrogen.

Variations in the electron conduction intensity may be attributed to conductive sp^2 nanoclusters (bright spots) distributed in a nonconductive sp^3 network (dark domains). The bright spots in the CAFM images of the annealed films [Figs. 5(d)–5(f)] are larger than those in the CAFM images of the as-deposited films [Figs. 5(a)–5(c)]. Since electron conduction occurs via sp^2 carbon bond configurations, the larger conducting spots seen in the CAFM images of the annealed *a*-C:H films reveal the presence of larger sp^2 clusters, which is consistent with the Raman spectroscopy results.

IV. CONCLUSIONS

Ultrathin *a*-C:H films deposited by PECVD were subjected to rapid (<1 s) thermal annealing to peak temperatures up to 660 °C in atmospheres of 80% N_2 and 20% O_2 to simulate the ambient environment in HAMR. Raman spectra demonstrated significant structural changes in 3.4-nm-thick *a*-C:H films above a critical peak annealing temperature of ~400–450 °C. XPS and XRR measurements did not reveal discernible changes in film thickness and sp^3 content due to RTA, indicating that oxidization and graphitization of the *a*-C:H films was secondary or negligible during RTA.

The red-shifting and the decrease of the FWHM of the G peak with the increase of the maximum annealing temperature above 450 °C suggested that hydrogen depletion, increase of sp^2 cluster size, and enhancement of carbon network ordering are the most likely factors affecting the structural stability of the *a*-C:H films. Although it is extremely difficult to quantify changes in the mechanical properties of such ultrathin films, the structural changes observed in this study provide indirect insight into the impact of RTA on the mechanical integrity of these films. For instance, an increase in the sp^2 cluster size may be interpreted as an increase in the film heterogeneity and, presumably, porosity, which are detrimental factors to the wear resistance of the *a*-C:H films.

The duration of a heating cycle in HAMR is on the order of a few nanoseconds. This implies that the RTA treatment used in the present study was more severe than that in HAMR. Consequently, it may

be argued that the structural stability of *a*-C:H films deposited on current hard disks by PECVD should be preserved, provided they are not heated to temperatures above ~400 °C during the read/write operation process of HAMR disk drives.

ACKNOWLEDGMENTS

This research was funded by the Computer Mechanics Laboratory, University of California, Berkeley and the UCB-KAUST Academic Excellence Alliance (AEA) Program. One of the authors (NW) would also like to acknowledge an internship during summer 2012 at HGST, a Western Digital Company, San Jose, California.

References

[1]H. Tsai and D. B. Bogy, J. Vac. Sci. Technol. A **5**, 3287 (1987).

[2]A. Grill, Surf. Coat. Technol. **94-95**, 507 (1997).

[3]J. Robertson, Mater. Sci. Eng. R **37**, 129 (2002).

[4]Z. Z. Bandić and R. H. Victora, Proc. IEEE **96**, 1749 (2008).

[5]M. H. Kryder, E. C. Gage, T. W. McDaniel, W. A. Challener, R. E. Rottmayer, G. Ju, Y.-T. Hsia, and M. F. Erden, Proc. IEEE **96**, 1810 (2008).

[6]W. A. Challener, C. Peng, A. V. Itagi, D. Karns, W. Peng, Y. Peng, X. Yang, X. Zhu, N. J. Gokemeijer, Y.-T. Hsia, G. Ju, R. E. Rottmayer, M. A. Seigler, and E. C. Gage, Nature Photon. **3**, 220 (2009).

[7]B. C. Stipe, T. C. Strand, C. C. Poon, H. Balamane, T. D. Boone, J. A. Katine, J.-L. Li, V. Rawat, H. Nemoto, A. Hirotsune, O. Hellwig, R. Ruiz, E. Dobisz, D. S. Kercher, N. Robertson, T. R. Albrecht, and B. D. Terris, Nature Photon. **4**, 484 (2010).

[8]N. Wang and K. Komvopoulos, IEEE Trans. Magn. **47**, 2277 (2011).

[9]Q. Ding, L. Wang, L. Hu, T. Hu, Y. Wang, and Y. Zhang, J. Appl. Phys. **109**, 013501 (2011).

[10]V. Kulikovsky, V. Vorlíček, P. Boháč, A. Kurdyumov, A. Deyneka, and L. Jastrabík, Diam. Relat. Mater. **12**, 1378 (2003).

[11]S. Takabayashi, K. Okamoto, H. Sakaue, T. Takahagi, K. Shimada, and T. Nakatani, J. Appl. Phys. **104**, 043512 (2008).

[12]D. S. Grierson, A. V. Sumant, A. R. Konicek, T. A. Friedmann, J. P. Sullivan, and R. W. Carpick, J. Appl. Phys. **107**, 033523 (2010).

[13]Z. L. Akkerman, H. Efstathiadis, and F. W. Smith, J. Appl. Phys. **80**, 3068 (1996).

[14]A. Grill, V. Patel, and B. S. Meyerson, J. Mater. Res. **5**, 2531 (1990).

[15]A. C. Ferrari, B. Kleinsorge, N. A. Morrison, A. Hart, V. Stolojan, and J. Robertson, J. Appl. Phys. **85**, 7191 (1999).

[16]J. Díaz, G. Paolicelli, S. Ferrer, and F. Comin, Phys. Rev. B **54**, 8064 (1996).

[17]S. Anders, J. Díaz, J. W. AgerIII, R. Y. Lo, and D. B. Bogy, Appl. Phys. Lett. **71**, 3367 (1997).

[18]M. Chhowalla, A. C. Ferrari, J. Robertson, and G. A. J. Amaratunga, Appl. Phys. Lett. **76**, 1419 (2000).

[19]N. M. J. Conway, A. Ilie, J. Robertson, W. I. Milne, and A. Tagliaferro, Appl. Phys. Lett. **73**, 2456 (1998).

[20]D. Wesner, S. Krummacher, R. Carr, T. K. Sham, M. Strongin, W. Eberhardt, S. L. Weng, G. Williams, M. Howells, F. Kampas, S. Heald, and F. W. Smith, Phys. Rev. B **28**, 2152 (1983).

[21]D. Wan and K. Komvopoulos, J. Phys. Chem. C **111**, 9891 (2007).

[22]M. Wormington, C. Panaccione, K. M. Matney, and D. K. Bowen, Phil. Trans. R. Soc. Lond. A **357**, 2827 (1999).

[23]L. G. Parratt, Phys. Rev. **95**, 359 (1954).

[24]L. Névot and P. Croce, Revue Phys. Appl. **15**, 761 (1980).

[25]M. Alam and Q. Sun, J. Mater. Res. **8**, 2870 (1993).

[26]A. C. Ferrari and J. Robertson, Phil. Trans. R. Soc. Lond. A **362**, 2477 (2004).

[27]A. C. Ferrari and J. Robertson, Phys. Rev. B **61**, 14095 (2000).

[28]A. C. Ferrari, S. E. Rodil, and J. Robertson, Phys. Rev. B **67**, 155306 (2003).

[29]J. O. Orwa, I. Andrienko, J. L. Peng, S. Prawer, Y. B. Zhang, and S. P. Lau, J. Appl. Phys. **96**, 6286 (2004).

[30]D. S. Knight and W. B. White, J. Mater. Res. **4**, 385 (1989).

[31]B. Bhushan, Diam. Relat. Mater. **8**, 1985 (1999).

[32]D. Liu and G. Benstetter, Appl. Surf. Sci. **249**, 315 (2005).

Table I. Current versus bias voltage applied to the AFM tip for as-deposited and annealed 3.4-nm-thick *a*-C:H films.

Tip bias voltage (V)	Root-mean-square current (pA)	
	as-deposited film	annealed film (660 ^{o}C)
0.0	0.648	0.512
0.2	93.7	71.8
1.0	1434	1249

List of Figures

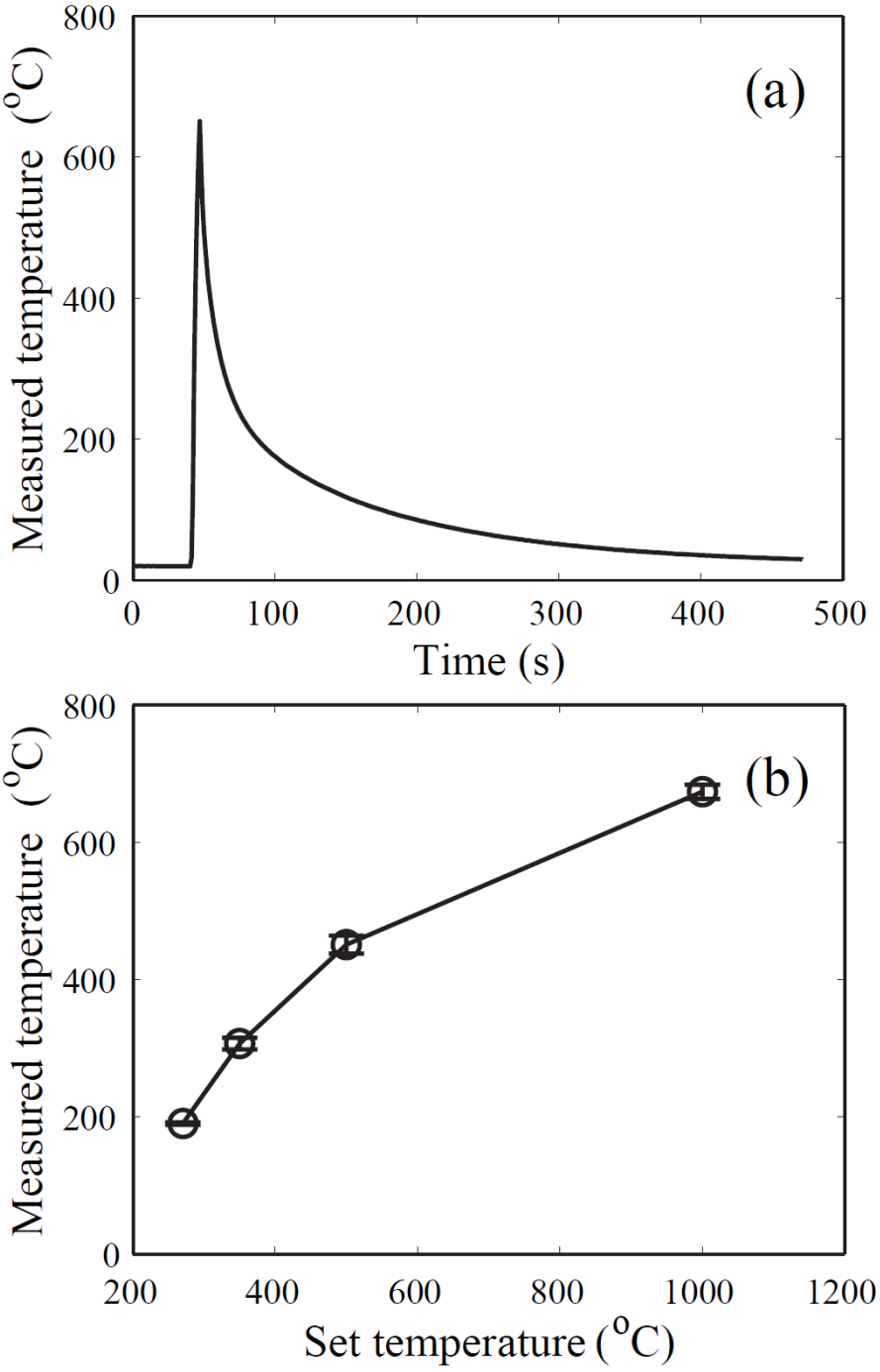
(a)
Measured temperature (°C)
800
600
400
200
0
0
100
200
300
400
500
Time (s)
(b)
Measured temperature (°C)
800
600
400
200
0
200
400
600
800
1000
1200
Set temperature (°C)

Figure 1

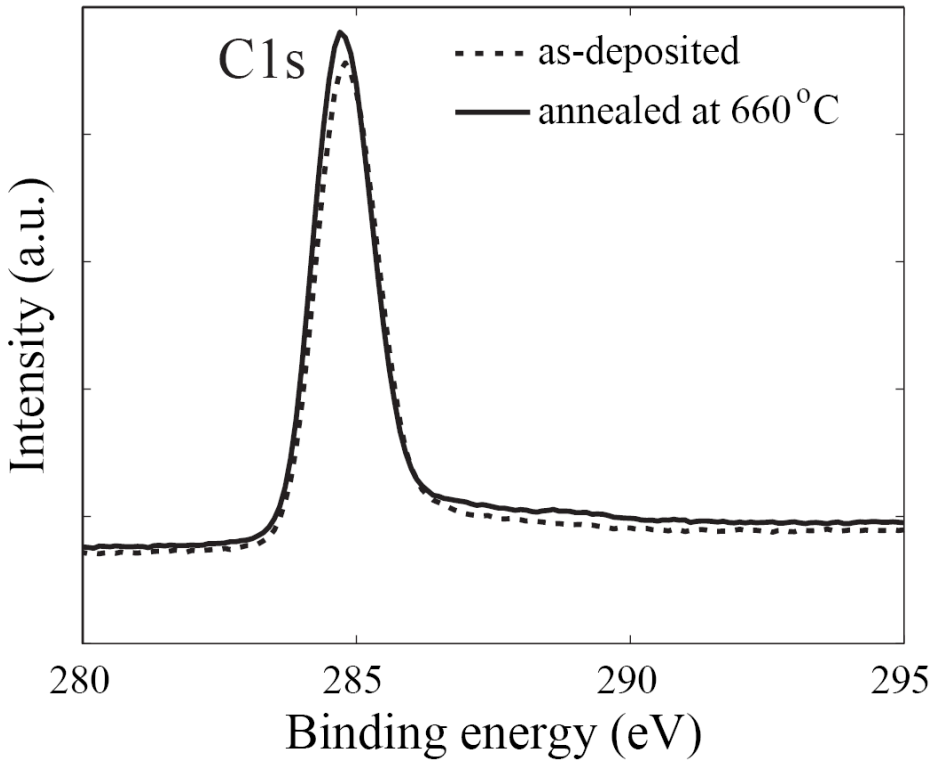
C1s
as-deposited
annealed at 660 °C
Intensity (a.u.)
280
285
290
295
Binding energy (eV)

Figure 2

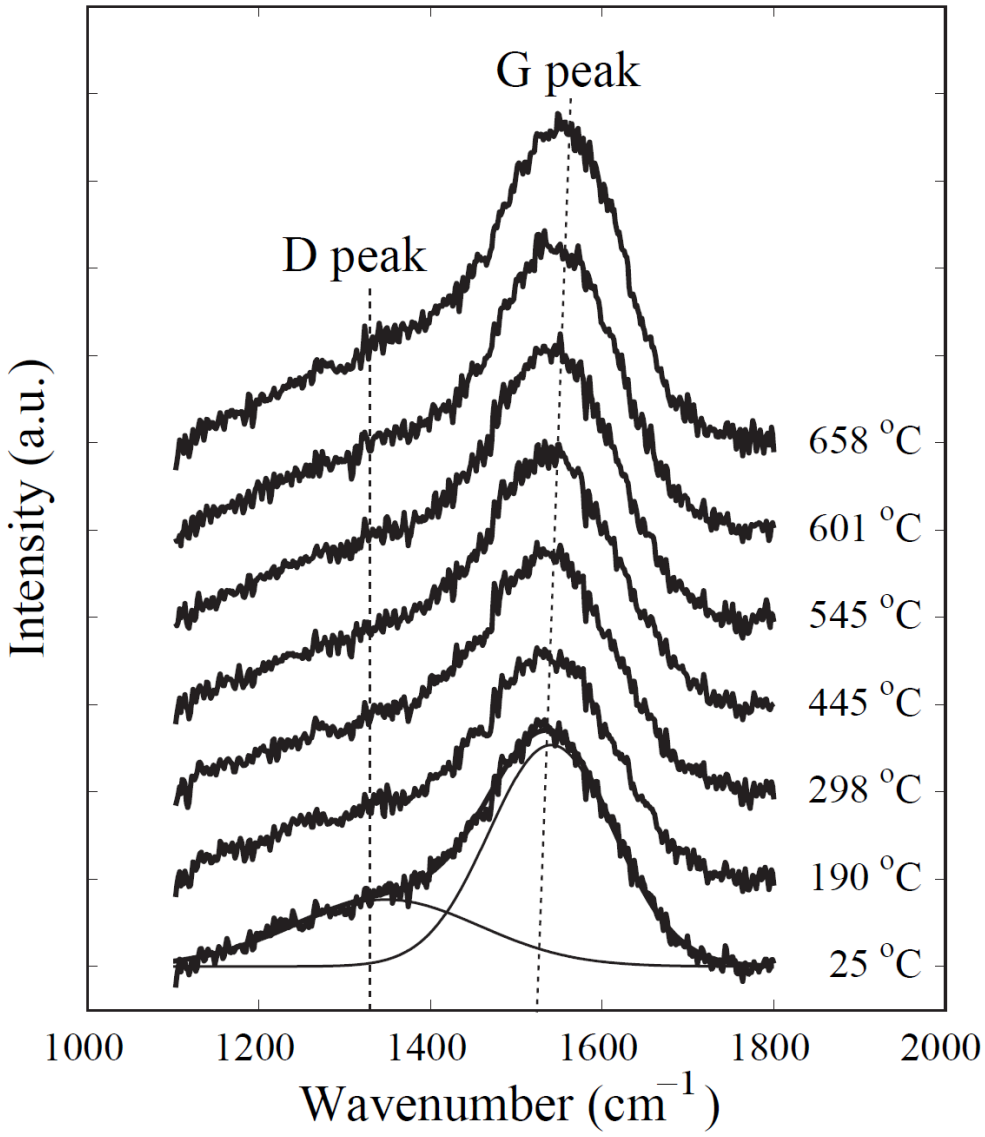
G peak
D peak
658 °C
601 °C
545 °C
445 °C
298 °C
190 °C
25 °C
Intensity (a.u.)
1000
1200
1400
1600
1800
2000
Wavenumber (cm^{-1})

Figure 3

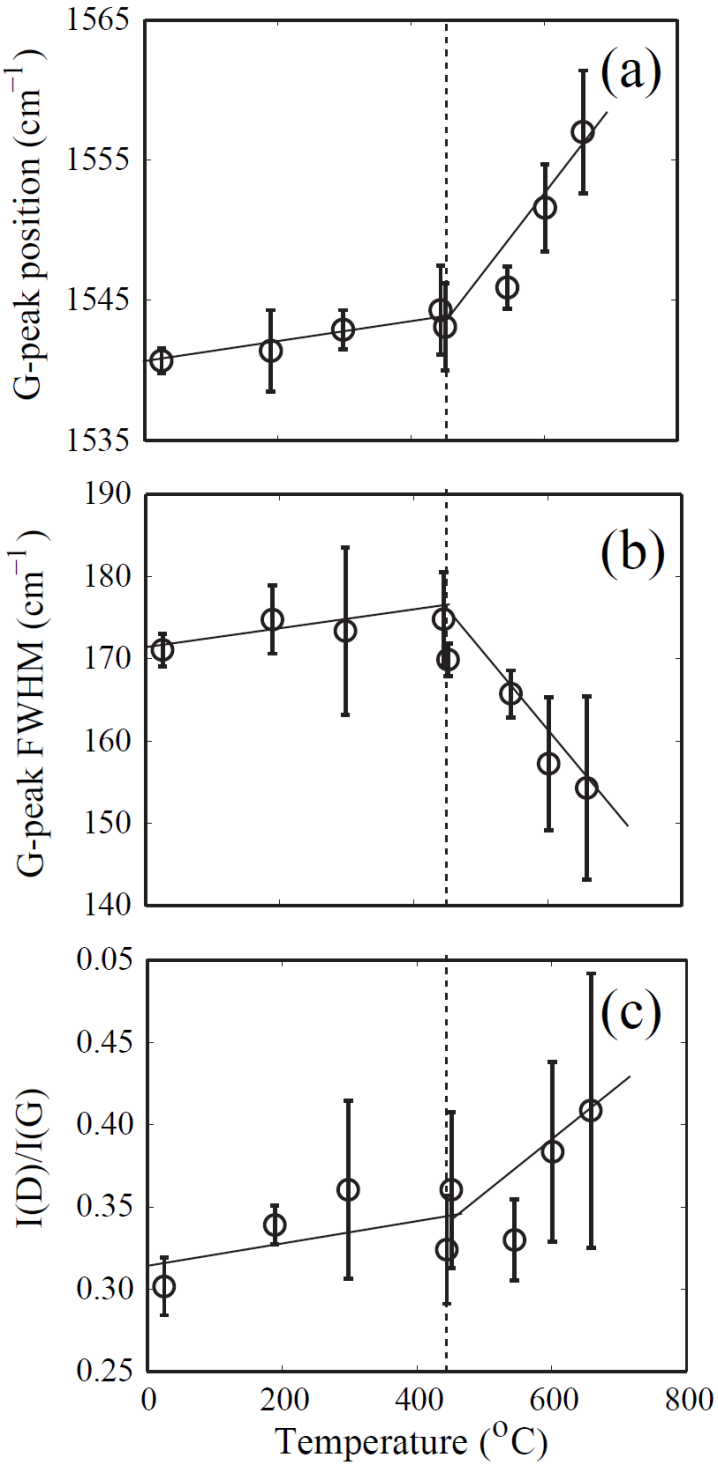
(a)
G-peak position (cm^{-1})
1565
1555
1545
1535
(b)
G-peak FWHM (cm^{-1})
190
180
170
160
150
140
(c)
I(D)/I(G)
0.05
0.45
0.40
0.35
0.30
0.25
0
200
400
600
800
Temperature (^{o}C)

Figure 4

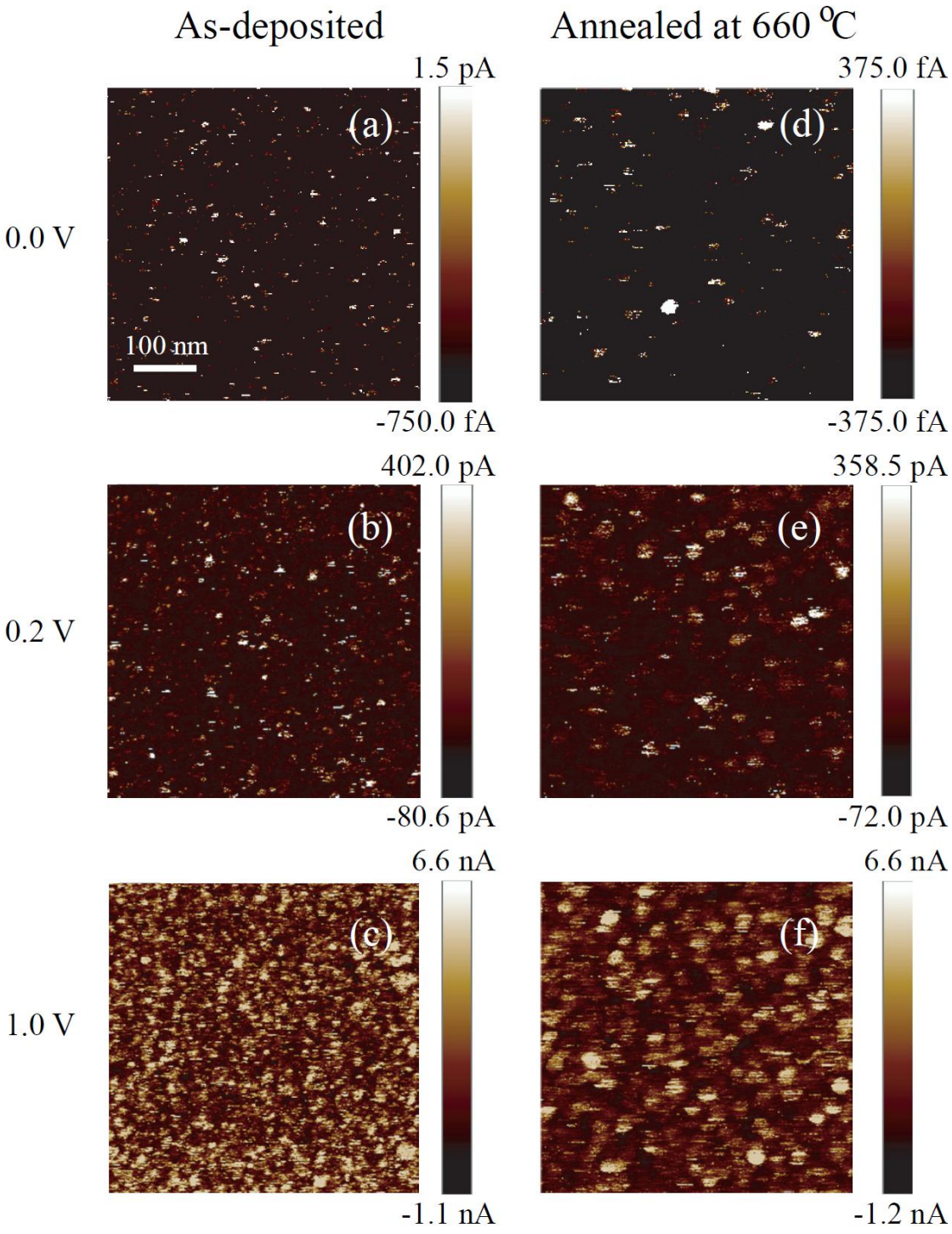
As-deposited
Annealed at 660 °C
1.5 pA
375.0 fA
0.0 V
(a)
(d)
100 nm
-750.0 fA
-375.0 fA
402.0 pA
358.5 pA
0.2 V
(b)
(e)
-80.6 pA
-72.0 pA
6.6 nA
6.6 nA
1.0 V
(c)
(f)
-1.1 nA
-1.2 nA

Figure 5